Inorganica Chimica Acta 482 (2018) 130–135

Contents lists available at ScienceDirect

Inorganica Chimica Acta

journal homepage: www.elsevier.com/locate/ica

Research paper

Synthesis, electrochemical/photophysical properties and computational investigation of 3,5-dialkyl BODIPY fluorophores

Yavuz Derin[a], Raşit Fikret Yılmaz[a], İbrahim Halil Baydilek[b], Vildan Enisoğlu Atalay[c,*], Abdil Özdemir[a], Ahmet Tutar[a,*]

[a] Sakarya University, Department of Chemistry, Faculty of Arts and Sciences, Sakarya 54187, Turkey
[b] Department of Medical Services and Techniques, Health Services Vocational School, Iğdır University, 76000 Iğdır, Turkey
[c] Üsküdar University, Department of Bioengineering, Istanbul 34662, Turkey

ARTICLE INFO

Keywords:
BODIPY
Fluorescence quantum yield
HOMO-LUMO
DFT

ABSTRACT

A series of 3,5 dimethyl and diethyl BODIPY with different substitutions at *meso* position are synthesized and characterized. Photophysical and electrochemical features of the 3,5 dialkyl BODIPY fluorophores are investigated using experimental and computational approaches. All fluorophores display absorption maxima around at 510 nm and emission maxima around at 520 nm which correspound to very narrow Stokes shift. Among the fluorophores, 3,5,8 alkylated BODIPYs are found to have high fluorescence quantum yield (1.00–0.93). 4-Bromophenyl group at *meso* position decreases fluorescence quantum yield of the dye while it increases with 4-methoxyphenyl group at *meso* position. The HOMO-LUMO energies of synthesized fluorophore compounds were calculated by B3LYP/6-31G(d,p) and B3LYP/6-311 + G(d,p) levels in chloroform phase. Electron donating and accepting groups show increasing and decreasing effect on the band gaps of the fluorophores respectively.

1. Introduction

Fluorescent dyes are of important place in many areas from clinical applications to technological applications [1]. Important class of these dyes is 4,4-difluoro-4-bora-3a,4a-diaza-s-indacene abbreviated as BODIPY and they have gained increasing attention, due to their excellent properties, for example chemical robustness, nearly insensitivity to polarity of the enviroment, good solubilty, intense absorption peak with high molar absoption coefficient in visible region, high fluorescence quantum yield and small Stokes shift [2–4]. In addition, these photophysical features can be easily tailored by different synthetic strategies on BODIPY core [5]. Thereby these dyes have many applications such as fluorescence probes [6–7], bio-labeling reagent [8], laser dyes [9], photo sentisizer for photodynamic therapy [10,11] and solar cell [12]. Photophysical and electrochemical behavior of BODIPY dyes are highly dependent upon the groups substituted to the structure. Some BODIPY derivatives such as dimethyl, tetramethyl BODIPY compounds were synthesized and relationship between the stuructures and properties was investigated [13,14].

In our present study, we carried out the synthesis of 3,5-dialkyl BODIPY fluorophores containing different substituents including ethyl (1), phenyl (2), 4-methoxyphenyl (3) and 4-bromophenyl (4) at *meso* position. Some of these dyes were reported in elsewhere nonetheless complete study of photophysical, electrochemical and computational investigation does not exist [14–18]. The relationship between structure and electronic properties of these fluorophores was investigated via experimental and computational approach.

2. Results and discussion

2.1. Spectroscopic properties of 3,5-dialkyl BODIPY fluorophores

^{1}H, ^{13}C and ^{19}F NMR spectroscopic methods were applied for characterization of all compounds (Fig. 1). For the final BODIPY compounds, NMR chemical shifts were computed by theoretical methods and compared with the experimental shifts so it is revealed that computed ^{1}H and ^{13}C chemical NMR shifts by GIAO method in $CDCl_3$ were best matched with the experimantal chemical shifts (Table S1). Fig. 2 shows that the absorption and emission spectra of the 3,5-dialkyl BODIPY fluorophores in CH_2Cl_2. The photophysical parameters of the fluorophores such as absorption maxima, molar extinction coefficient, emission maxima, Stokes shift and quantum yield were summarized in Table 1. Maximum absorption peaks of the fluorophores were located between the range of 508 and 515 nm, as for their emission maximas,

* Corresponding authors.
E-mail addresses: vildan.enisoglu@uskudar.edu.tr (V.E. Atalay), atutar@sakarya.edu.tr (A. Tutar).

https://doi.org/10.1016/j.ica.2018.06.006
Received 5 April 2018; Received in revised form 24 May 2018; Accepted 4 June 2018

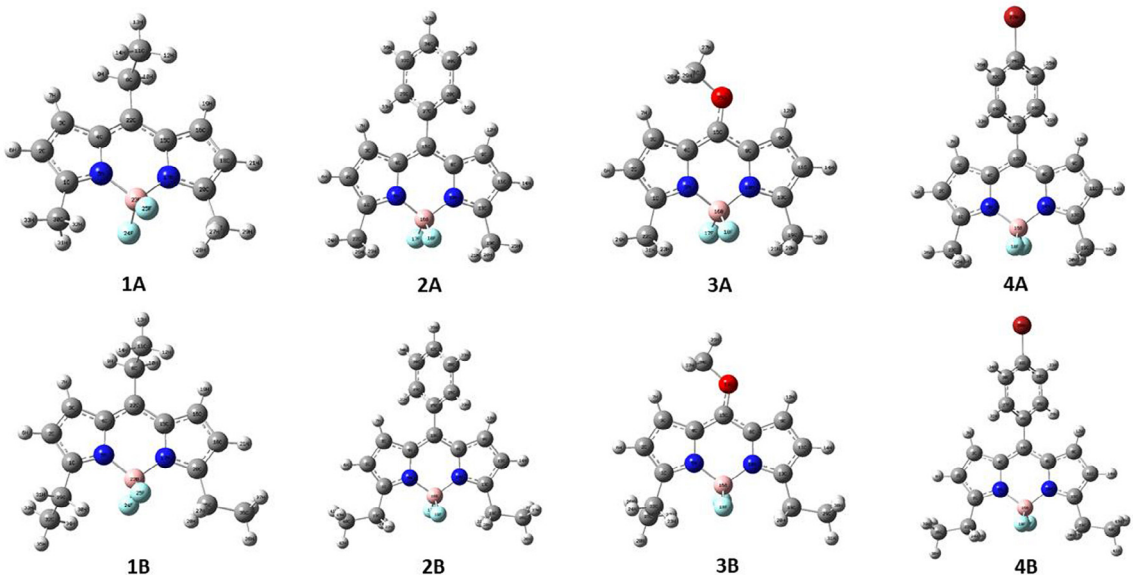

Fig. 1. Synthesized fluorophore molecules.

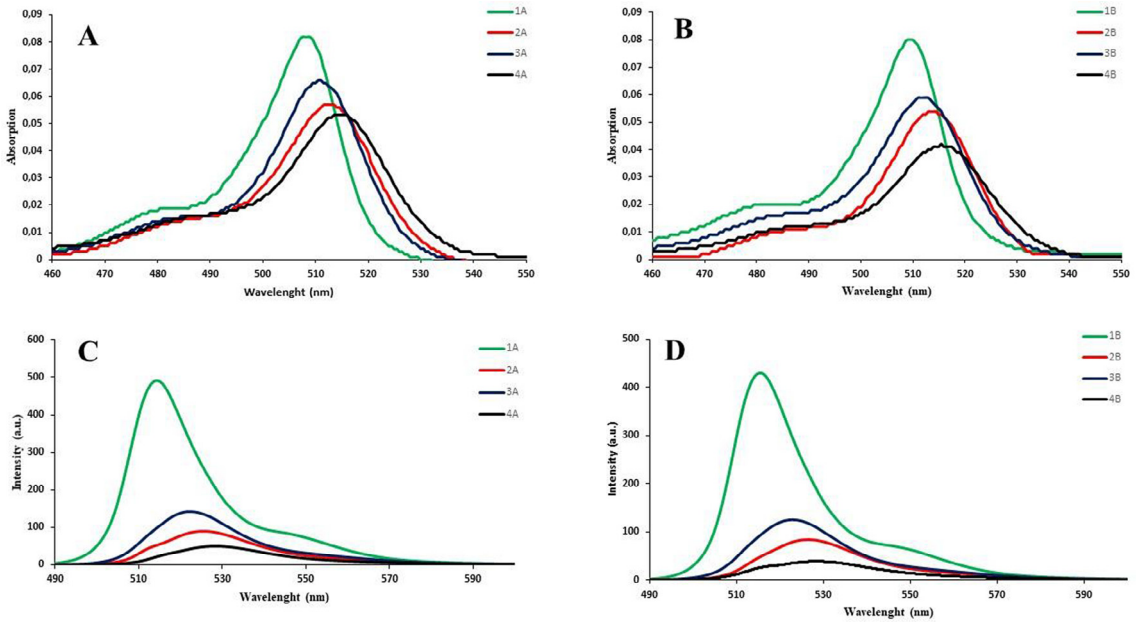

Fig. 2. The electronic absorption (A and B) and fluorescence spectra (C and D) of the 3,5-dialkyl BODIPY fluorophores **1A–4B** in dilute solution in $CHCl_3$.

Table 1
Photophysical properties of 3,5-dialkyl BODIPY fluorophores (**1A–4B**) in $CHCl_3$ solvent.

Compound	λ_{abs} (nm)	λ_{em} (nm)	$\Delta\lambda$ (nm)[a] Stokes Shift	φ[b]	ε[c]
1A	508	514	6	1.00	6.8×10^4
2A	512	525	13	0.36	5.7×10^4
3A	511	522	11	0.45	7.1×10^4
4A	514	529	15	0.24	6.6×10^4
1B	509	515	6	0.93	7.3×10^4
2B	514	526	12	0.37	5.8×10^4
3B	512	523	11	0.51	7.0×10^4
4B	515	528	13	0.25	5.6×10^4

[a] Stokes Shift (nm).
[b] Fluorescence quantum yield.
[c] Molar absorption coefficient ($mol \cdot L^{-1} \cdot cm^{-1}$).

they ranged between 514 and 529 nm. The fluorophores show strong absorption peaks around at 510 nm and a shoulder located at higher energy side (approximately 480 nm) attributed to S_0-S_1 and the 0–1 vibrational transitions, respectively. This peaks are similar for structurally typical BODIPY fluorophores [19]. The fluorophores can be categorised into two groups according to *meso* position and 3,5 positions. The dye couples having same group at *meso* position and methyl (**1A–4A**) or ethyl (**1B–4B**) at 3,5 positions differ from each other only ~1–2 nm in absorption and emission spectra. The reason for the small difference value in absorption and emission spectra is due to similar electronic effects of methyl and ethyl groups on the core BODIPY structure [20].

It is obvious that the fluorophores (**1A–1B**) bearing alkyl group at *meso* position showed the highest fluorescence quantum yield (~1.00–0.93) and the smallest Stokes shift. However it is worth noting that the fluorophores bearing phenyl ring at *meso* position drastically decreased the fluorescence quantum yield with respect to fully

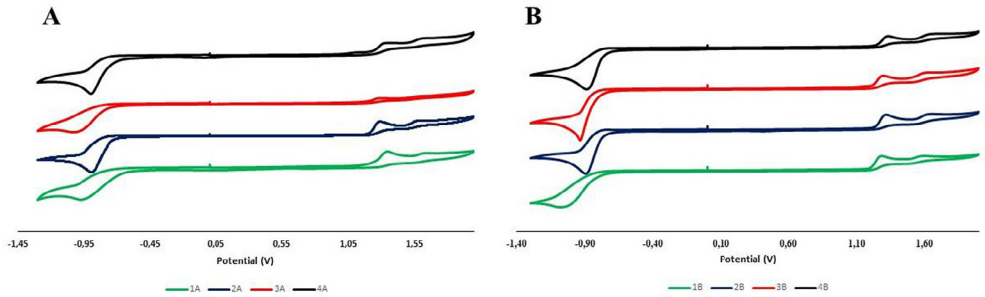

Fig. 3. The cyclic voltametry of the 3,5-dialkyl BODIPY fluorophores **1A–4B** in dilute solution in CH_3CN containing 0.1 M TBAPF6 at a scan rate of 100 mV/s.

alkylated fluorophores in the series. 4-methoxy phenyl which serves as electron donating group resulted in somewhat higher quantum yield and smaller Stokes shift. On the other hand 4-bromophenyl as electron accepting group led to low quantum yield steaming from heavy atom effect of the bromine atom [21,22] and larger Stokes shift among the phenyl bearing fluorophores. The fluorophores with methoxy and bromine containing phenyl ring exhibit hypsochromic and bathochromic shift with respect to only phenyl possessing counterparts, respectively.

2.2. Electrochemistry properties

Cyclic voltammetry (CV) is frequently utilized to measure electrochemical properties of the dyes from which the highest occupied molecular orbital (HOMO) and the lowest unoccupied molecular orbital (LUMO) energy levels are predicted. The cyclic voltammograms were recorded for the fluorophores (**1A–4B**) and depicted in Fig. 3.

The HOMO energies are directly related to the ionization potential, LUMO energies are directly related to the electron affinity. The energy and distribution of the HOMO-LUMO orbitals energy difference between HOMO-LUMO gap orbital are an important stability for structures [23]. Also HOMO-LUMO and band gap values of the fluorophores calculated via experimental and theoretical methods were gathered in Table 2. A molecule with a small gap is more polarized and is known as soft molecule. More importantly, the HOMO orbitals are mainly localized on the nitrogen-containing five-membered ring, whereas the LUMO orbitals are distributed over the whole molecules. This means that pyrrole ring in 3,5-dialkyl BODIPY fluorophores (**1A–4B**) would be more easily attacked. All fluorophores have similar CV profiles which consist of an irreversible reduction and oxidation peak appeared at around 0.9 V and 1.30 V, respectively. For all fluorophores, it appears that HOMO energies are almost same however, the band gaps and LUMO energies are different. It can be clearly stated that electron accepting groups lead to narrow band gap on the other hand electron donating groups widen the band gap [24,25]. The order of stability of the fluorophore compounds is **4B** < **4A** < **2B** < **2A** < **1A** ≈ **1B** < **3B** < **3A** as obtained by theoretical methods. As a result 4-bromophenyl groups decreased the band gap as in the fluorophores **4A–4B**, 4-methoxyphenyl groups caused to the wide band gap in the fluorophore couples **3A–3B**. Although ethyl groups at *meso* posion (**1A–1B**) are electron donating groups, considerable change was not observed in the band gap which is found very similar to phenyl bearing ones (**2A–2B**).

Finaly, theoretical HOMO-LUMO and band gap energies (in Fig. 4) of the fluorophore 3,5 dimethylBODIPY **(1A–4A)** and diethylBODIPY **(1B–4B)** were found to have same trend compared to the experimental values.

Table 2
Calculated (B3LYP/6-311 + G(d.p)) and experimental HOMO-LUMO values (eV) and band gaps levels in $CHCl_3$ phase.

Compounds	Theoretical			Experimental		
	HOMO	LUMO	Band Gap	HOMO	LUMO	Band Gap
1A	−5.61	−2.58	3.03	−5.59	−3.25	2.34
1B	−5.60	−2.57	3.03	−5.56	−3.22	2.34
2A	−5.64	−2.67	2.97	−5.56	−3.22	2.34
2B	−5.63	−2.67	2.96	−5.59	−3.24	2.33
3A	−5.65	−2.30	3.35	−5.54	−3.19	2.35
3B	−5.52	−2.29	3.23	−5.57	−3.22	2.35
4A	−5.70	−2.75	2.95	−5.59	−3.28	2.31
4B	−5.68	−2.75	2.93	−5.59	−3.27	2.32

3. Conclusions

In this study firstly, all compounds are successfully synthesized by given methods and structurely charecterized by ^1H, ^{13}C, ^{19}F NMR spectroscopy methods. Our study reveals the effect of substituated phenyl groups at *meso* position and alkyl groups on photophysical properties such as fluorescence quatum yield, absorption/emission maxima, Stokes shift, molar absorption coefficient. In this respect, The fluorophores (**1A–1B**) bearing alkyl group instead of phenyl groups at *meso* position are found to show highest quantum yields (1.00–0.93) which can be good candidate for quantum yield standart. On the other hand, the absorption and emission spectrum profiles of the fluorophores are bearly influenced from phenyl groups but slightly effected from alkyl group at *meso* position. Cyclic voltammetry in combination with UV–vis spectrophotometry is applied to investigate electrochemical properties of the fluorophores such as HOMO-LUMO energy levels and band gap. Alkyl groups (methyl and ethyl) at 3,5 position lead to almost no change on electrochemical properties which may be due to similar electronic effect of methyl and ethyl. It is observed that band gap gets wide introducing electron accepting group namely 4-bromophenyl to *meso* position and remains nearly unchanged in ethyl, phenyl, 4-methoxyphenyl bearing fluorophores at *meso* position.

4. Experimental and theoretical section

4.1. General methods of synthesis

Thin layer chromatography was carried out on Merck silica F_{254} 0.255 mm plates, and spots were visualized by UV at 254 nm. Flash column chromatography was performed using Merck 60 (70–230 mesh) silica gel. Melting points were taken on a MPM-H1 capillary melting points apparatus. Solvents were concentrated at reduced pressure. IR spectra were recorded on a Shimadzu Prestige-21 (200 VCE) FT/IR instrument. ^1H (300 MHz), ^{13}C (75 MHz) and ^{19}F (282 MHz) NMR spectra in $CDCl_3$ were obtained on a Varian Infinity Plus spectrometer. 2-methyl-1*H*-pyrrole (**B1**) and 2-ethyl-1*H*-pyrrole (**B2**) were synthesized by modification of the method given in the literature [26,27].

4.1.1. Synthesis of 2-methyl-1H-pyrrole *B1*

Two-necked reaction balloon (250 mL); ethyleneglycol (80 mL), KOH (8 g, 142 mmol), hydrazinehydrate ($N_2H_4{\cdot}H_2O$), (6 mL,

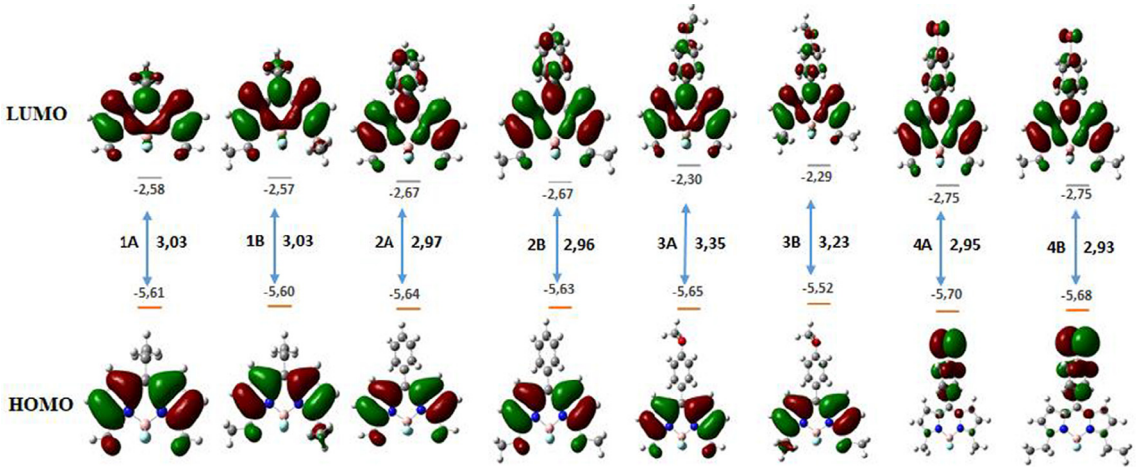

Fig. 4. The HOMO-LUMO energies of **1A–4B** and bandgaps are in eV.

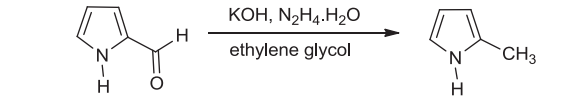

Fig. 5. Synthesis of 2-methyl-1*H*-pyrrole **B1**.

0.12 mmol) and pyrrole-2-carboxyaldehyde (1H-pyrrole-2-carbaldehyde) (4 g, 42 mmol) were added at room temperature under nitrogen. The reaction balloon was placed in the jacketed heater and the temperature control probe and the other neck reflux system were placed. The temperature controller was heated for 15 min at 80 °C then brought to 130 °C and stirred for 15 min. (After 30 min, the mixture was further refluxed for 3 h at 180 °C) . After 3 h, the temperature was turned off and the temperature of there action medium was reduced to 50 °C. The reflux of there action system, which cooled to 50 °C, was removed, replacing the small distillate bridge and collection adapter on the distillate bridge, 25 mL collection bubbles on both ends of the adapter, and the distillate bridge connected to the vacuum device. The system was turned on and the temperature was raised slowly. When the temperature reached 88.4 °C, the reaction mixture started to boil. The first distillate came to the collection balloon at 90 °C. The distillate was collected for 35 min and the temperature slowly began to fall. Then the temperature and vacuum were turned off. The distillate from the system was extracted with diethylether (3 × 20 mL) and dried over Na_2SO_4 to remove the excess solvent under reduced vacuum (light yellow liquid, 2.51 g, % 73), (Fig. 5). ^{1}H NMR ($CDCl_3$, 300 MHz, ppm) δ_H 7.92 (bs, 1H, N—H), 6.69 (s, 1H, Pi-H), 6.16 (t, J = 2.6 Hz, 1H, Pi-H), 5.94 (d, J = 2.5 Hz, 1H, Pi-H), 2.31 (s, 3H, —CH_3). ^{13}C NMR ($CDCl_3$, 75 MHz, ppm) δ_C 128.0, 116.7, 108.7, 106.1, 13.2. FT-IR (cm^{-1}): 3376, 3097, 2916, 1684, 1571, 1457, 1412, 1269, 1117, 1094, 1025, 951, 884, 782, 707.

4.1.2. Synthesis of 2-ethyl-1H-pyrrole **B2**

Two-necked reaction balloon (250 mL); ethyleneglycol (100 mL), KOH (10 g, 177.5 mmol), hydrazinehydrate ($N_2H_4{\cdot}H_2O$), (8 mL, 0.16 mmol) and methyl-2-pyrrole ketone (5 g, 45 mmol) were added at room temperature under nitrogen. The reaction balloon was placed in the jacketed heater and the temperature control probe and the other neck reflux system were placed. The temperature controller was heated for 15 min at 100 °C then brought to 150 °C and stirred for 15 min. After 30 min, the temperature was further refluxed for 5 h at 200 °C. After 5 h, the temperature was turned off and the temperature of the reaction medium was reduced to 50 °C. The reflux of the reaction system, which cooled to 50 °C, was removed, replacing the small distillate bridge and collection adapter on the distillate bridge, 25 mL collection bubbles on both ends of the adapter, and the distillate bridge connected to the vacuum device. The system was turned on and the temperature was raised slowly. When the temperature reached 92 °C, the reaction mixture started to boil. The first distillate came to the collection balloon at 97 °C. The distillate was collected for 47 min and the temperature slowly began to fall. Then the temperature and vacuum were turned off. The distillate from the system was extracted with diethylether (3 × 20 mL) and dried over Na_2SO_4 to remove the excess solvent under reduced vacuum (light yellow liquid, 3.11 g, % 64), (Fig. 6). ^{1}H NMR ($CDCl_3$, 300 MHz, ppm) δ_H 7.98 (bs, 1H, N—H), 6.82 (s, 1H, Pi-H), 6.38 (t, J = 2.8 Hz, Pi-H), 6.17 (s, 1H, Pi-H), 2.80 (q, J = 2.4 Hz, 2H, —CH_2), 1.45 (t, J = 2.8 Hz 3H, —CH_3). ^{13}C NMR ($CDCl_3$, 75 MHz, ppm) δ_C 134.5, 116.5, 108.4, 104.4, 21.1, 13.9. FT-IR (cm^{-1}): 3381, 3100, 2967, 1875, 1685, 1630, 1568, 1459, 1326, 1209, 1117, 1096, 1022, 932, 883, 794, 707.

4.2. General procedure for 3,5-dialkyl BODIPY fluorophores (**1A–4B**)

To a solution of substituted pyrrole (2 eq.) in $C_2H_4Cl_2$ (40 mL) was dropwise added a solution of acylchloride (1 eq.) at room temperature under nitrogen. After addition, the solution was stirred at 120 °C for 16 h under nitrogen. The solution was cooled to 0 °C ice-water bath, triethylamine (5 eq.) was then added dropwise at 0 °C for 10 min, and the mixture was stirred for 10 min (Fig. 7). The ice-water bath was removed. After reaction mixture was reached to room temperature, then $BF_3.OEt_2$ (10 eq.) was added, and the mixture was stirred at room temperature for 20 h. After removal of solvent, the residue was passed through a silica gel column using 25% CH_2Cl_2 in hexanes to give BODIPY as crystalline product after removal of solvent.

4.2.1. Synthesis of 4,4-difluoro-8-ethyl-3,5-dimethyl-4-bora-3a,4a-diaza-s-indacene (**1A**)

Green powder (400 mg, 28%, isolated yield); m.p = 182–184 °C; R_f (25% Hexane/EtOAc) = 0.57. ^{1}H NMR ($CDCl_3$, 300 MHz, ppm) δ_H 7.09 (d, J = 4.1 Hz, 2H, Pi-H), 6.27 (d, J = 4.1 Hz, 2H, Pi-H), 2.83 (q, J = 7.7 Hz, 2H, —CH_2—), 2.60 (s, 6H, —CH_3), 1.37 (t, J = 7.7 Hz, 3H, —CH_3). ^{13}C NMR ($CDCl_3$, 75 MHz, ppm) δ_C 158.8, 147.1, 134.5, 126.8,

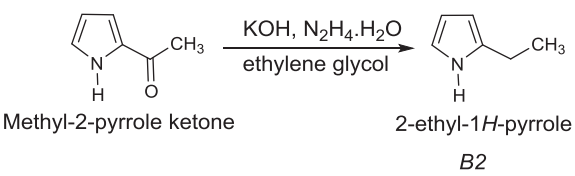

Fig. 6. Synthesis of 2-ethyl-1*H*-pyrrole **B2**.

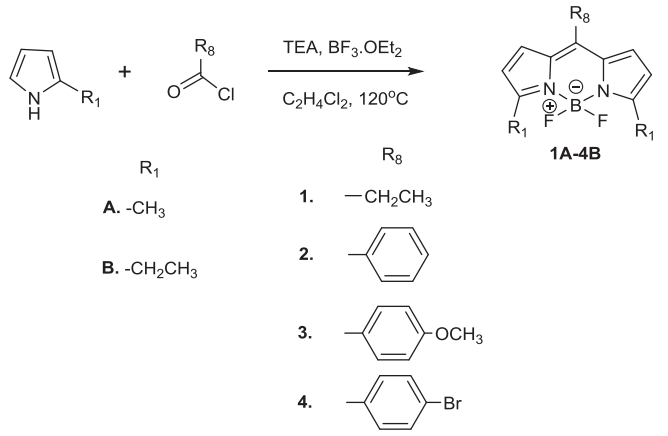

Fig. 7. General synthesis scheme of 3,5-dialkyl BODIPY (**1A–4B**).

119.0, 23.9, 18.4, 15.0. ^{19}F NMR (CDCl3, 282 MHz, ppm) δ_F −148.65 (q, J_{BF} = 33.76 Hz) FT-IR (cm^{-1}): 2967, 2922, 2858, 1727, 1572, 1493, 1456, 1373, 1286, 1241, 1146, 1097, 999, 958, 909, 784, 717, 664. MALDI-TOF-MS *m/z* calcd. for $C_{13}H_{15}BF_2N_2$ [M]$^+$: 248.1296; found: 248.1474.

*4.2.2. Synthesis of 4,4-difluoro-8-ethyl-3,5-diethyl-4-bora-3a,4a-diaza-s-indacene (**1B**)*

Orange powder (400 mg, 25%, isolated yield); m.p = 135–137 °C; R_f (50% Hexane/$CHCl_3$) = 0.18. ^{1}H NMR ($CDCl_3$, 300 MHz, ppm) δ_H 7.13 (d, *J* = 4.2 Hz, 2H, Pi-H), 6.34 (d, *J* = 4.2 Hz, 2H, Pi-H), 3.04 (q, *J* = 7.6 Hz, 4H, −CH_2−), 2.82 (q, *J* = 9.0 Hz, 2H, −CH_2−), 1.35 (m, *J* = 7.6 Hz, 3H, −CH_3), 1.30 (t, *J* = 9.0 Hz, 6H, −CH_3). ^{13}C NMR ($CDCl_3$, 75 MHz, ppm) δ_C 162.8, 147.5, 134.2, 126.8, 116.9, 23.9, 22.2, 18.4, 13.0. ^{19}F NMR (CDCl3, 282 MHz, ppm) δ_F −146.45 (q, J_{BF} = 33.81 Hz) FT-IR (cm^{-1}): 2971, 2937, 2877, 1565, 1486, 1437, 1316, 1241, 1131, 1101, 1026, 965, 803, 736, 713. MALDI-TOF-MS *m/z* calcd. for $C_{15}H_{19}BF_2N_2$ [M + H]$^+$: 277.1688; found: 277.1691.

*4.2.3. Synthesis of 4,4-difluoro-8-phenyl-3,5-dimethyl-4-bora-3a,4a-diaza-s-indacene (**2A**)*

Bright green crystal (400 mg, 28%, isolated yield); m.p = 110–112 °C; R_f (50% Hexane/EtOAc) = 0.67. ^{1}H NMR ($CDCl_3$, 300 MHz, ppm) δ_H 7.49–7.46 (m, 5H, Ar-H), 6.70 (d, *J* = 4.1 Hz, 2H, Pi-H), 6.26 (d, *J* = 4.1 Hz, 2H, Pi-H), 2.66 (s, 6H, −CH_3). ^{13}C NMR ($CDCl_3$, 75 MHz, ppm) δ_C 157.8, 142.8, 134.7, 134.3, 130.7, 130.6, 130.2, 128.4, 119.6, 15.2. ^{19}F NMR (CDCl3, 282 MHz, ppm) δ_F −147.95 (q, J_{BF} = 33.51 Hz) FT-IR (cm^{-1}): 2975, 2850, 1738, 1576, 1538, 1493, 1437, 1395, 1260, 1218, 1135, 1064, 981, 879, 781, 717. MALDI-TOF-MS *m/z* calcd. for $C_{17}H_{15}BF_2N_2$ [M]$^+$: 296.1296; found: 296.1237.

*4.2.4. Synthesis of 4,4-difluoro-8-phenyl-3,5-diethyl-4-bora-3a,4a-diaza-s-indacene (**2B**)*

Orange-green crystal (400 mg, 25%, isolated yield); m.p = 155–157 °C; R_f (50% Hexane/EtOAc) = 0.71. ^{1}H NMR ($CDCl_3$, 300 MHz, ppm) δ_H 7.50–7.47 (m, 5H, Ar-H), 6.75 (d, *J* = 4.2 Hz, 2H, Pi-H), 6.36 (d, *J* = 4.2 Hz, 2H, Pi-H), 3.10 (q, *J* = 7.6 Hz, 4H, −CH_2−), 1.35 (t, *J* = 7.6 Hz, 6H, −CH_3). ^{13}C NMR ($CDCl_3$, 75 MHz, ppm) δ_C 163.7, 143.1, 134.4, 130.7, 130.6, 130.2, 129.1, 128.4, 117.5, 22.3, 13.1. ^{19}F NMR (CDCl3, 282 MHz, ppm) δ_F −145.45 (q, J_{BF} = 33.64 Hz) FT-IR (cm^{-1}): 2971, 2922, 2850, 1735, 1550, 1489, 1429, 1369, 1312, 1282, 1128, 1090, 977, 883, 788, 720, 645, 592. MALDI-TOF-MS *m/z* calcd. for $C_{19}H_{19}BF_2N_2$ [M]$^+$: 324.1609; found: 324.1940.

*4.2.5. Synthesis of 4,4-difluoro-8-(4-methoxyphenyl)-3,5-dimethyl-4-bora-3a, 4a-diaza-s-indacene (**3A**)*

Red crystal (500 mg, 21%, isolated yield); m.p = 188–190 °C; R_f (50% Hexane/EtOAC) = 0.54. ^{1}H NMR ($CDCl_3$, 300 MHz, ppm) δ_H 7.45 (d, *J* = 8.8 Hz, 2H, Ar-H), 7.00 (d, *J* = 8.8 Hz, 2H, Ar-H), 6.76 (d, *J* = 4.1 Hz, 2H, Pi-H), 6.28 (d, *J* = 4.1 Hz, 2H, Pi-H), 3.89 (s, 3H, −OCH_3), 2.64 (s, 6H, −CH_3). ^{13}C NMR ($CDCl_3$, 75 MHz, ppm) δ_C 157.2, 134.7, 132.4, 131.2, 130.5, 126.8, 119.4, 113.9, 113.7, 55.7, 15.1. ^{19}F NMR (CDCl3, 282 MHz, ppm) δ_F −147.95 (q, J_{BF} = 33.00 Hz) FT-IR (cm^{-1}): 3111, 3019, 2971, 2922, 2850, 1739, 1599, 1573, 1547, 1491, 1446, 1374, 1250, 1218, 1136, 1074, 1026, 960, 882, 840, 784, 762, 739, 713, 589, 527. MALDI-TOF-MS *m/z* calcd. for $C_{18}H_{17}BF_2N_2O$ [M]$^+$: 326.1402; found: 326.1281.

*4.2.6. Synthesis of 4,4-difluoro-8-(4-methoxyphenyl)-3,5-diethyl-4-bora-3a,4a-diaza-s-indacene (**3B**)*

Orange-yellow crystal (460 mg, 25%, isolated yield); m.p = 136–138 °C; R_f (50% Hexane/$CHCl_3$) = 0.13. ^{1}H NMR ($CDCl_3$, 300 MHz, ppm) δ_H 7.47 (AA′ part of AA′BB′, 2H, Ar-OCH_3), 7.01 (BB′ part of AA′BB′, 2H, Ar-OCH_3), 6.78 (d, *J* = 3.9 Hz, 2H, Pi-H), 6.36 (d, *J* = 3.9 Hz, 2H, Pi-H), 3.90 (s, 3H, −OCH_3), 3.08 (q, *J* = 7.5 Hz, 4H, −CH_2−), 1.35 (t, *J* = 7.5 Hz, 6H, −CH_3). ^{13}C NMR ($CDCl_3$, 75 MHz, ppm) δ_C 163.2, 161.4, 143.2, 134.4, 132.3, 130.6, 126.9, 117.3, 113.9, 55.7, 22.2, 13.1 ^{19}F NMR (CDCl3, 282 MHz, ppm) δ_F −145.70 (q, J_{BF} = 33.50 Hz). FT-IR (cm^{-1}): 2970, 2938, 2876, 1605, 1573, 1550, 1508, 1488, 1433, 1319, 1280, 1250, 1215, 1175, 1127, 1087, 1022, 999, 980, 882, 833, 758, 736, 706, 644, 589. MALDI-TOF-MS *m/z* calcd. for $C_{20}H_{21}BF_2N_2O$ [M]$^+$: 354.2077; found: 354.2034.

*4.2.7. Synthesis of 4,4-difluoro-8-(4-bromophenyl)-3,5-dimethyl-4-bora-3a,4a-diaza-s-indacene (**4A**)*

Red powder (390 mg, 21%, isolated yield); m.p = 180–182 °C; R_f (50% Hexane/$CHCl_3$) = 0.15. ^{1}H NMR (300 MHz, $CDCl_3$, ppm): δ_H 7.62 (AA′ part of AA′BB′, 2H, Ar-H), 7.37 (BB′ part of AA′BB′, 2H, Ar-H), 6.68 (d, *J* = 4.2 Hz, 2H, Pi-H), 6.28 (d, *J* = 4.2 Hz, 2H, Pi-H), 2.65 (s, 6H, −CH_3). ^{13}C NMR (75 MHz, $CDCl_3$): δ_C 158.3, 141.1, 134.5, 133.2, 132.0, 131.8, 130.4, 124.7, 120.0, 15.2. ^{19}F NMR (CDCl3, 282 MHz, ppm) δ_F −148.05 (q, J_{BF} = 33.94 Hz) FT-IR (cm^{-1}): 3140, 2925, 2858, 1738, 1572, 1550, 1535, 1452, 1373, 1264, 1215, 1140, 1073, 986, 877, 828, 795, 765, 731, 652, 580. MALDI-TOF-MS *m/z* calcd. for $C_{17}H_{14}BBrF_2N_2$ [M + H]$^+$: 375.0480; found: 375.0468.

*4.2.8. Synthesis of 4,4-difluoro-8-(4-bromophenyl)-3,5-diethyl-4-bora-3a,4a-diaza-s-indacene (**4B**)*

Red powder (230 mg, 23%, isolated yield); m.p = 138–139 °C; R_f (50% Hexane/$CHCl_3$) = 0.20. ^{1}H NMR (300 MHz, $CDCl_3$): δ_H 7.68 (AA′ part of AA′BB′, 2H, Ar-H), 7.30 (BB′ part of AA′BB′, 2H, Ar-H), 6.67 (d, *J* = 4.2 Hz, 2H, Pi-H), 6.34 (d, *J* = 4.2 Hz, 2H, Pi-H), 3.06 (q, *J* = 7.6 Hz, 4H, −CH_2−), 1.33 (t, *J* = 7.6 Hz, 6H, −CH_3). ^{13}C NMR (75 MHz, $CDCl_3$): δ_C 164.2, 141.4, 134.1, 133.2, 132.0, 131.7, 130.4, 124.7, 117.8, 22.3, 13.0. ^{19}F NMR (CDCl3, 282 MHz, ppm) δ_F −145.45 (q, J_{BF} = 33.49 Hz) FT-IR (cm^{-1}): 3095, 2964, 2501, 2196, 2049, 1915, 1762, 1693, 1569, 1551, 1486, 1462, 1435, 1403, 1389, 1341, 1312, 1255, 1219, 1120, 1080, 1067, 1035, 1006, 978, 881, 797, 769, 757, 731, 699. MALDI-TOF-MS *m/z* calcd. for $C_{19}H_{18}BBrF_2N_2$ [M + H]$^+$: 403.0793; found: 403.1129.

4.3. Photophysical and electrochemical measurements

All absorption and fluorescence spectra were acquired from diluted solution of BODIPY compunds in CH_2Cl_2 using Shimadzu UV-2600 UV–VIS spectrophotometer and Hitachi F-7000 Fluorescence spectrophotometer respectively. The absorbance at excitation wavelenght was kept below 0.1. Fluorescence quantum yields were calculated from the equation given below [28]. Rhodamine B solution in ethanol was used as reference dye (φ_r = 0.49) [29].

$$\varphi_s = \varphi_r \left(\frac{I_{smp}}{I_{ref}}\right)\left(\frac{A_{ref}}{A_{smp}}\right)\left(\frac{\mu_{smp}}{\mu_{ref}}\right)^2$$

The subscripts *ref* and *smp* reffer to the reference and sample dyes. φ is the fluorescence quantum yield; I is the area under fluorescence spectrum; A is the absorption of light at excitation wavelenght; μ is refraxtive index of the solvents (Ethanol and CH_2Cl_2).

Cyclic voltammetric (CV) studies were carried out on Gamry Interphase 1000 potentiostat with an electrochemical system utilizing a three-electrode configuration consisting of a platinum electrode, platinum wire electrode and a silver/silver chloride electrode as working electrode, counter electrode, and reference electrode, respectively. The electrochemical behaviors of BODIPY dyes were investigated in CH_3CN containing 0.1 M tetrabutylammonium hexafluorophosphate (TBAPF6) as supporting electrolyte at a scan rate of 100 mV/s.

HOMO is calculated via oxidation peak potential, while band gap is calculated from absorption onset wavelenght using the given equations. Therefore LUMO can be obtained from these two values of E_{HOMO} and E_g. The potentials were calibrated with ferrocene redox couple (Fc/Fc^+) [30,32].

$$E_{HOMO} = -(E[oxvsFc/Fc^+] + 4.8)eV$$

$$E_g = 1240/\lambda_{onset}$$

$$E_{LUMO} = E_{HOMO} - E_g$$

4.4. Computational methods

Conformational searches were performed for eight different compounds synthesized with semi-emprical PM6 method [33,34] by using the Spartan'16 v1.1.4 [35]. The obtained most stable conformer structures each compound were optimized with semi-emprical PM6 method in the gas phase and Density Functional Theory (DFT) B3LYP (Becke's Three Parameter Hybrid Functional using the Lee, Yang and Parr Correlation Functional) [36] with 6-31G(d,p) basis set in the gas phase and in the dichloroethane solvent with the IEF-PCM approach. To determine the HOMO-LUMO energies were calculated using time-dependent density functional theory (TD-DFT) at the B3LYP/6-31G(d,p) and B3LYP/6-311 + G(d,p) levels in chloroform phase was done by using the Self-Consistent Reaction Field (SCRF) method. DFT/B3LYP has been reported as a method to calculate BODIPY's HOMO-LUMO orbital energies in the literature [37,38]. Chemical shifts (δ, ppm) of the synthesized compounds (**1A–4B**) were computed by using DFT/B3LYP/6-31Gdp method with the Continuous Set of Gauge Transformations (CSGT) approach [39–41] and the Gauge-Independent Atomic Orbital (GIAO) [42,43] method for all compounds in gas and deuterated chloroform ($CDCl_3$) phases. All of the visualizations and calculations were carried out by the methods implemented in GaussView5.0 [44] and Gaussian 09 package [45].

Acknowledgements

We are grateful to İlkay Şişman for running the cyclic voltammetry. This work was financially supported by the Scientific and Technological Research Council of Turkey (TUBITAK) (Grant Number 114Z176). Sakarya University Scientific Research Foundation [Project no. 2014-02-04-010].

Appendix A. Supplementary data

Supplementary data associated with this article can be found, in the online version, at http://dx.doi.org/10.1016/j.ica.2018.06.006.

References

[1] R.M. Christie, Rev. Prog. Color. Relat. Top. 23 (1993) 1–18.
[2] G. Ulrich, R. Ziessel, A. Harriman, Angew. Chem. Int. Ed. 47 (2008) 1184–1201.
[3] A. Louder, K. Burgess, Chem Rev. 107 (2007) 4891–4932.
[4] T.V. Goud, A. Tutar, J.F. Biellmann, Tetrahedron 62 (2006) 5084–5091.
[5] N. Boens, V. Leen, W. Dehaen, Chem. Soc. Rev. 41 (2012) 1130–1172.
[6] R. Ziessel, G. Ulrich, A. Harriman, New J. Chem. 31 (2007) 496–501.
[7] W. Qin, W. Dou, V. Leen, W. Dehaen, M.V. Auweraer, N. Boens, RSC Adv. 6 (2016) 7806–7816.
[8] S. Niu, C. Massif, G. Ulrich, P.Y. Renard, A. Romieu, R. Ziessel, Chem. Eur. J. 18 (2012) 7229–7242.
[9] T.G. Pavlopoulos, J.H. Boyer, K. Thangaraj, G. Sathyamoorthi, M.L. Soong, Appl. Opt. 31 (1992) 7089–7094.
[10] M.J. Ortiz, A.R. Agarrabeitia, G.D. Sampedro, B.J. Prieto, T.A. Lopez, W.A. Massad, H.A. Montejano, A.G. Norman, I.L. Arbeloa, J. Tetrahedron. 68 (4) (2012) 1153–1162.
[11] Y. Cakmak, S. Kolemen, S. Duman, Y. Dede, Y. Dolen, B. Kilic, Z. Kostereli, L.T. Yildirim, A.L. Dogan, D. Guc, E.U. Akkaya, Angew. Chem. Int. Ed. 50 (2011) 11937–11941.
[12] H. Klfout, A. Stewart, M. Elkhalifa, H. He, ACS Appl. Mater. Interfaces 9 (2017) 39873–39889.
[13] Y. Chen, L. Wan, D. Zhang, Y. Bian, J. Jiang, Photochem. Photobiol. Sci. 10 (2011) 1030–1038.
[14] W. Qin, M. Baruah, M.V. Auweraer, F.C.D. Schryver, N. Boens, J. Phys. Chem. A. 109 (2005) 7371–7384.
[15] D.J. Kimball, S. Raut, P.L. Jameson, W.N. Smith, Z. Gryczynski, V.S. Dzyuba, RSC Adv. 5 (2015) 19508–19511.
[16] E. Lager, J. Liu, A. Aguilar-Aguilar, B.Z. Tang, E. Peña-Cabrera, J. Org. Chem. 74 (5) (2009) 2053–2058.
[17] J.Y. Shin, K. Kim, J.M. Lim, T. Tanaka, D. Kim, K. Kim, H. Shinokubo, A. Osuka, Chem. Eur. J. 20 (2014) 4574–4582.
[18] W.N. Smith, A. Alonso, C.M. Brown, V.S. Dzyuba, Biochem. Biophys. Res. Commun. 391 (2010) 1455–1458.
[19] Y. Yu, L. Jiao, J. Wang, H. Wang, C. Yu, E. Haoa, N. Boens, Chem. Commun. 53 (2017) 581.
[20] C. Hansch, A. Leo, R.W. Taft, Chem. Rev. 91 (1991) 165–195.
[21] L. Jiao, W. Pang, J. Zhou, Y. Wei, X. Mu, G. Bai, E. Hao, J. Org. Chem. 76 (2011) 9988–9996.
[22] S.H. Lim, C. Thivierge, P.N. Sliwinska, J. Han, H. Bergh, G. Wagnières, K. Burgess, H.B. Lee, J. Med. Chem. 53 (2010) 2865–2874.
[23] J. Aihara, J. Phys. Chem. A 103 (1999) 7487–7495.
[24] S. Berson, S. Cecioni, M. Billon, Y. Kervella, R. Bettignies, S. Bailly, S. Guillerez, Sol. Energy Mater. Sol. Cells 94 (2010) 699–708.
[25] P. Matlaba, T. Nyokong, Polyhedron 21 (2002) 2463–2472.
[26] T.D. Lash, D.T. Richter, C.M. Shiner, J. Org. Chem. 64 (1999) 7973–7982.
[27] M.M.C. Lo, G.C. Fu, J. Am. Chem. Soc. 124 (2002) 4572–4573.
[28] K. Rurack, M. Spieles, Anal. Chem. 83 (2011) 1232–1242.
[29] K.G. Casey, E.L. Quitevis, J. Phys. Chem. 92 (1988) 6590–6594.
[30] J. Liao, Y. Wang, Y. Xu, H. Zhao, X. Xiao, X. Yang, J. Tetrahedron 71 (2015) 5078–5084.
[31] S.P. Economopoulos, C.L. Chochos, H.A. Ioannidou, M. Neophytou, C. Charilaou, G.A. Zissimou, J.M. Frost, T. Sachetan, M. Shahid, J. Nelson, M. Heeney, D.D.C. Bradley, G. Itskos, P.A. Koutentis, S.A. Choulis, RSC Adv. 3 (2013) 10221–10229.
[32] A. Günsel, E. Güzel, A.T. Bilgiçli, I. Şişman, M.N. Yarasir, J. Photochem. Photobiol. A 348 (2017) 57–67.
[33] J.J.P. Stewart, J. Mol. Model. 14 (2008) 499–535.
[34] J.J.P. Stewart, J. Mol. Model. 15 (2009) 765–805.
[35] Spartan'16. Wavefunction, Inc., Irvine, CA.
[36] C. Lee, W. Yang, R.G. Parr, Phys. Rev. B 37 (1988) 785–789.
[37] D. Hu, T. Zhang, S. Li, T. Yu, X. Zhang, R. Hu, J. Feng, S. Wang, T. Liang, J. Chen, N.L. Sobenina, A.B. Trofimov, Y. Li, J. Ma, G. Yang, Nat. Commun. 9 (2018) 362.
[38] J. Wang, Q. Wu, Y. Xu, C. Yu, Y. Wei, X. Mu, E. Hao, L. Jiao, RSC Adv. 6 (2016) 52180–52188.
[39] T.A. Keith, R.F.W. Bader, Chem. Phys. Lett. 194 (1992) 1–8.
[40] T.A. Keith, R.F.W. Bader, Chem. Phys. Lett. 210 (1993) 223–231.
[41] J.R. Cheeseman, G.W. Trucks, T.A. Keith, M.J.J. Frisch, Chem. Phys. 104 (1996) 5497–5509.
[42] F. London, J. Phys. Radium 8 (1937) 397–409.
[43] K. Wolinski, J.F. Hilton, P. Pulay, J. Am. Chem. Soc. 112 (1990) 8251–8260.
[44] GaussView, Version 5, Dennington R, Keith T, Millam J. Semichem Inc., Shawnee Mission KS, 2009.
[45] M.J. Frisch, G.W. Trucks, H.B. Schlegel, G.E. Scuseria, M.A. Robb, J.R. Cheeseman, J.A. Montgomery, J.T. Vreven, K.N. Kudin, J.C. Burant, J.M. Millam, S.S. Iyengar, J. Tomasi, V. Barone, B. Mennucci, M. Cossi, G. Scalmani, N. Rega, G.A. Petersson, H. Nakatsuji, M. Hada, M. Ehara, K. Toyota, R. Fukuda, J. Hasegawa, M. Ishida, T. Nakajima, Y. Honda, O. Kitao, H. Nakai, M. Klene, X. Li, J.E. Knox, H.P. Hratchian, J.B. Cross, C. Adamo, J. Jaramillo, R. Gomperts, R.E. Stratmann, O. Yazyev, A.J. Austin, R. Cammi, C. Pomelli, J.W. Ochterski, P.Y. Ayala, K. Morokuma, G.A. Voth, P. Salvador, J.J. Dannenberg, V.G. Zakrzewski, A.D. Daniels, O. Farkas, A.D. Rabuck, K. Raghavachari, J.V. Ortiz, "Gaussian 09", Gaussian, Inc., Pittsburgh PA.